# Dependence of the high-latitude thermospheric densities on the interplanetary magnetic field

Y.-S. Kwak,[1] A. D. Richmond,[2] Y. Deng,[2,3] J. M. Forbes,[4] and K.-H. Kim[1,5]

Received 5 November 2008; revised 13 February 2009; accepted 27 February 2009; published 12 May 2009.

[1] The systematic analysis of the interplanetary magnetic field (IMF) $B_y$ and $B_z$ influences on observed thermospheric density is presented. For this purpose, the high-latitude southern summer thermospheric total mass density near 400 km altitude, derived from the high-accuracy accelerometer on board the Challenging Minisatellite Payload (CHAMP) spacecraft, is statistically analyzed in magnetic coordinates. The difference density distributions, which are obtained by subtracting values for zero IMF from those for nonzero IMF, vary strongly with respect to the direction of the IMF: Difference densities for negative $B_y$ show significant enhancements in the early morning hours and hours around dawn but show reduced values in the dusk sector. For positive $B_y$ the difference densities are opposite in sign to those for negative $B_y$. Density differences for negative $B_z$ show significant increases in the cusp region and premidnight sector but a small decrease in the dawn sector. The difference densities at high latitudes tend to be weakest when $B_z$ is positive. We suggest that the high-latitude thermospheric density variations for different IMF conditions, especially in the dawn and dusk sectors, can be strongly determined by thermospheric winds, which are associated with the ionospheric convection and vary strongly with respect to the IMF direction. We also suggest that density variations, especially in auroral and cusp regions, are also influenced by the local heating associated with ionospheric currents, which vary with IMF conditions.

**Citation:** Kwak, Y.-S., A. D. Richmond, Y. Deng, J. M. Forbes, and K.-H. Kim (2009), Dependence of the high-latitude thermospheric densities on the interplanetary magnetic field, *J. Geophys. Res.*, *114*, A05304, doi:10.1029/2008JA013882.

## 1. Introduction

[2] Thermospheric density is important not only for predicting the atmospheric drag in the context of satellite ephemeris prediction, but also in understanding the thermosphere-ionosphere coupling process as well. Since magnetic storms and substorms cause significant changes in the compositional distribution of the thermosphere, the thermosphere responses to the ensuing geomagnetic activity have been the topic of a number of papers [e.g., *Mayr and Volland*, 1973; *Prölss*, 1980; *Miller et al.*, 1990; *Burns et al.*, 1991, 1995a, 1995b; *Fuller-Rowell et al.*, 1994, 1996; *Forbes et al.*, 1996; *Liu and Lühr*, 2005; *Sutton et al.*, 2005; *Bruinsma et al.*, 2006].

[3] The direction and strength of the interplanetary magnetic field (IMF) exert strong influences on the high-latitude ionospheric plasma convection and current [e.g., *Heppner*, 1972; *Heppner and Maynard*, 1987; *Foster et al.*, 1986; *Ruohoniemi and Greenwald*, 1996; *Weimer*, 1995, 2001], so it is generally believed that they influence the high-latitude thermospheric wind [e.g., *McCormac and Smith*, 1984; *McCormac et al.*, 1985, 1991; *Killeen et al.*, 1985, 1995; *Meriwether and Shih*, 1987; *Thayer et al.*, 1987; *Rees and Fuller-Rowell*, 1989, 1990; *Sica et al.*, 1989; *Hernandez et al.*, 1991; *Niciejewski et al.*, 1992, 1994; *Won*, 1994; *Richmond et al.*, 2003], forcing on the wind [*Kwak and Richmond*, 2007; *Kwak et al.*, 2007] and Joule/particle heating [e.g., *McHarg et al.*, 2005; *Zhang et al.*, 2005]. From the relationship between the IMF and the thermospheric wind and heating, we can expect that the thermospheric density driven by the high-latitude forcing and heating is also strongly modulated by the IMF variation. *Crowley et al.* [2006] investigated the effect of IMF $B_y$ on thermospheric composition at 140 and 200 km at high and middle latitudes in northern hemisphere through numerical experiments. Their simulations showed that a clockwise rotation of the ionospheric convection pattern resulting from a change from $B_y$-negative to $B_y$-positive drives a corresponding rotation in the wind, neutral density, and composition distributions.

[4] To date, no systematic analysis of observed IMF influences, which include effects of $B_z$ component as well as $B_y$ component, on the thermospheric density has been carried out. This is the subject of this study. For this

[1]Division of Space Astronomy, Korea Astronomy and Space Science Institute, Daejeon, South Korea.
[2]High Altitude Observatory, National Center for Atmospheric Research, Boulder, Colorado, USA.
[3]Now at CIRES, University of Colorado and Space Weather Prediction Center, NOAA, Boulder, Colorado, USA.
[4]Department of Aerospace Engineering Sciences, University of Colorado, Boulder, Colorado, USA.
[5]Now at Department of Astronomy and Space Science, Kyung Hee University, Yongin City, South Korea.


0148-0227/09/2008JA013882$09.00

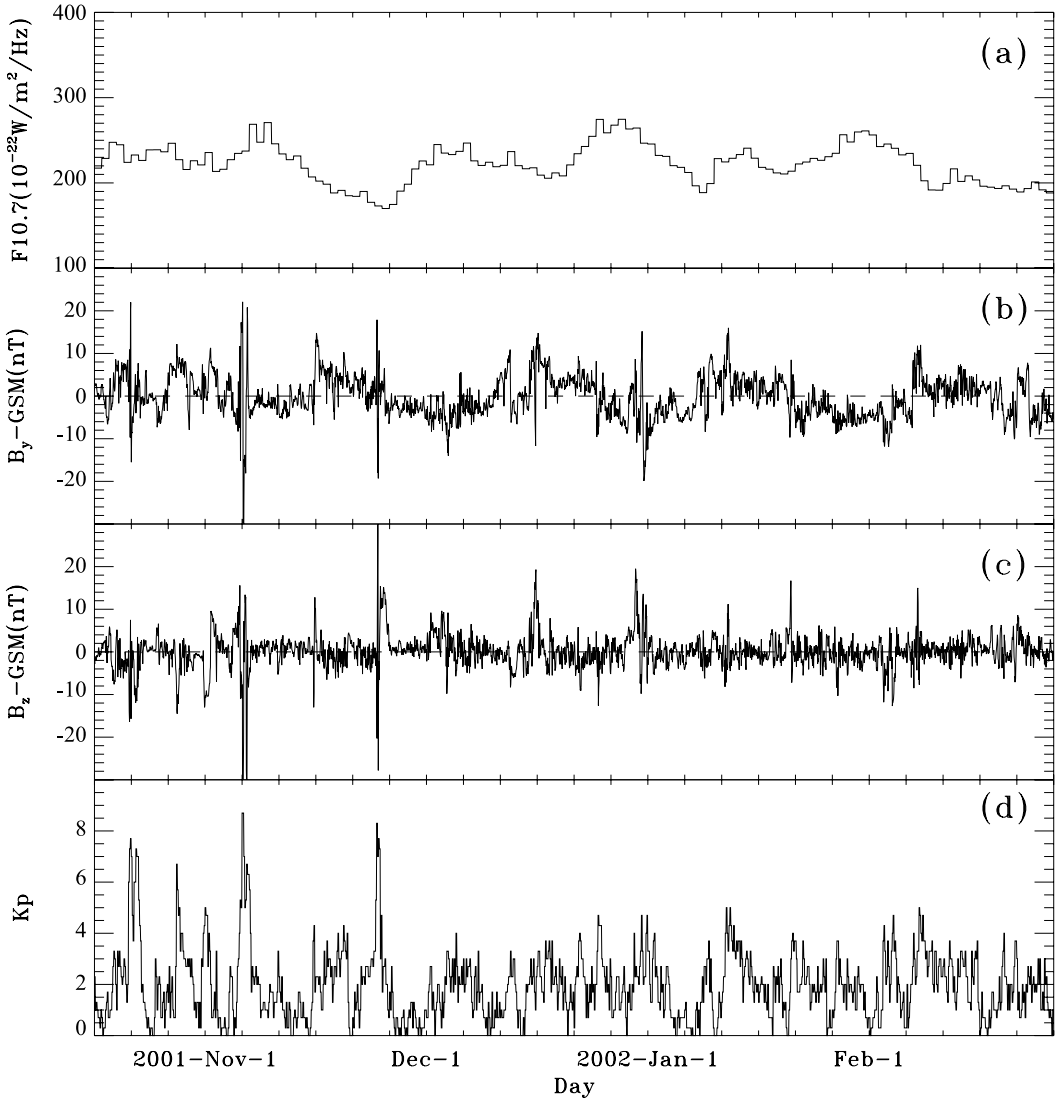


**Figure 1.** Variations of (a) solar EUV flux proxy, F10.7 (in units of $10^{-22}$ W m$^{-2}$ Hz$^{-1}$), the hourly IMF (b) $B_y$ and (c) $B_z$ values, and (d) Kp index during 17 October 2001 through 24 February 2002.

purpose, the high-latitude thermospheric total mass density around 400 km altitude, derived from the high-accuracy accelerometer on board the Challenging Minisatellite Payload (CHAMP) spacecraft during 17 October 2001 through 24 February 2002, is statistically analyzed in magnetic coordinates as a function of the direction and strength of the IMF for southern summer hemisphere.

## 2. Data Analyses

[5] In this study, we use total mass density measurements from accelerometers on board CHAMP to interpret the response of the thermosphere to the IMF. The data for the present study come from the period during the southern summer of 17 October 2001 to 24 February 2002 centered on the December solstice. During this period, CHAMP was in a near-circular high-inclination orbit, precessing in local time at a rate of 5.6 min per day and providing approximate measurements of total mass density along the orbit with 10s resolution. Eventually CHAMP covered almost all magnetic latitudes and magnetic local times during this study period of 131 days. Along-track axis data are used for density calculations. The derivation of thermosphere densities from these data involves consideration of such effects as radiation pressure, satellite shape and orientation, thruster firings, etc.. The detailed procedure for deriving thermospheric total mass densities from the CHAMP accelerometer has been described by *Sutton et al.* [2007]. Density variations due to changes in orbital altitude (the CHAMP orbit altitude ranges from 390 km to 460 km) have been removed via normalization to a common altitude of 400 km using the NRLMSISE-00 thermospheric density model [*Picone et al.*, 2002]. All the quantities are then converted into Quasi-Dipole (QD) coordinates (QD-latitude and magnetic local time (MLT)) [*Richmond*, 1995].

[6] Omission of winds in the process of deriving the thermospheric densities from in-track accelerations generally causes errors in the derived densities. *Bruinsma et al.* [2004] found that density errors due to neglect of zonal winds ranged from 4% per 100 m s$^{-1}$ at the equator to 0% near the poles and that errors due to neglect of meridional

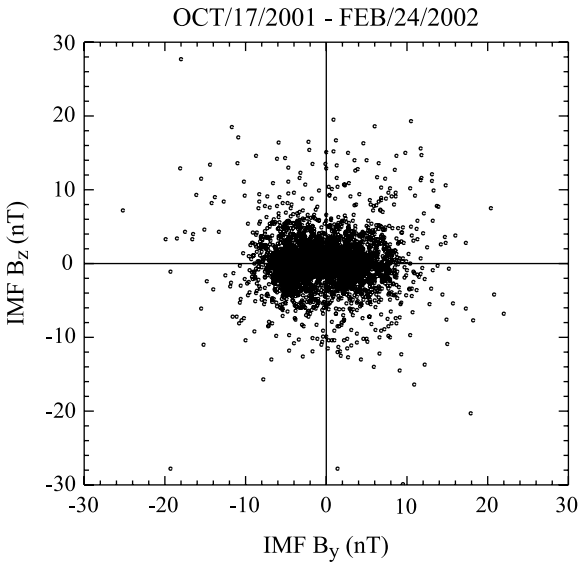


**Figure 2.** Distributions of the hourly IMF $B_y$ and $B_z$ values during 17 October 2001 to 24 February 2002.

winds ranged from 2% at the equator to 5% per 100 m $s^{-1}$ near the poles. Under strongly geomagnetic disturbed conditions, these errors can be high at high latitudes, where large thermospheric winds exist.

[7] In addition, we use hourly values of the IMF $B_y$ (positive duskward) and $B_z$ (positive northward) components in Geocentric Solar-Magnetospheric (GSM) coordinates from the National Space Science Data Center (NSSDC) OMNIWeb (http://nssdc.gsfc.nasa.gov/omniweb). Figure 1 shows the distribution of the IMF $B_y$ and $B_z$ components with the solar EUV flux proxy, F10.7 and Kp index, for 17 October 2001 to 24 February 2002. As shown in Figure 2, the IMF values during this study period are distributed evenly, allowing us to investigate effects of different IMF conditions on the thermospheric density.

[8] It is expected that changes in the thermospheric neutral density are lagged behind changes in the IMF due to inertia of the air. Therefore, the densities are correlated with lagged, time-averaged IMF values. The lagged time-averaged IMF $B_y$ and $B_z$ components are defined as

$$\overline{B}_{[y,z]}(t,\tau) = \frac{\int_0^t B_{[y,z]}(t')e^{(t'-t)/\tau}dt'}{\int_0^t e^{(t'-t)/\tau}dt'} \quad (1)$$

where the IMF $B_y$ and $B_z$ components $B_{[y,z]}(t)$ are treated as continuous functions of time $t$ and where $\tau$ is the effective averaging and lag time for the exponential weighting function in the integrands. We use a value for $\tau$ of 1.5 h at 400 km, which is estimated by considering the energy in the $\overline{B}_y$-dependent and $\overline{B}_z$-dependent components of the fitted density in a manner similar to that used by *Richmond et al.* [2003]. By using the entire data set, we integrate the energy in this component over the area poleward of −57.5° QD latitude for different values of $\tau$, and search for values of $\tau$ that tend to maximize the integrated energy.

[9] In this study, we classify the entire data set into five overlapping subsets, similar to those used by *Richmond et al.* [2003]. For each subset a linear regression of the data with respect to $\overline{B}_y$ and $\overline{B}_z$ is performed, and then the regression relation is evaluated for reference values of $\overline{B}_y$ and $\overline{B}_z$. Table 1 lists IMF reference values and selection criteria for the data subsets. Subset 1 represents when the magnitudes of the IMF are small, for which the reference values of $\overline{B}_y$ and $\overline{B}_z$ are zero. The magnitudes of the nonzero reference values of $\overline{B}_y$ and $\overline{B}_z$ for subsets 2–5, that is, 4.4 nT and 3.4 nT, respectively, are their respective root-mean-square (RMS) values for the entire data set when the time constant $\tau$ = 1.5 h. Figure 3 shows the distribution of CHAMP observations versus MLT with intervals of 10° from −90° to −50° latitude for the five subsets. The average values of F10.7 are 214, 219, 208, 215 and 214 for the five subsets, that is, for IMF 0, IMF $\overline{B}_y(-)$, IMF $\overline{B}_y(+)$, IMF $\overline{B}_z(-)$ and IMF $\overline{B}_z(+)$, respectively.

## 3. Effect of the IMF on the Thermospheric Density Variations

[10] In this section the high-latitude thermospheric density distributions for different IMF orientations are addressed. Figure 4 shows the average high-latitude thermospheric total mass density distributions at 400 km over the southern summer hemisphere for Subset 1 (zero IMF) from CHAMP data. As for Figures 5 and 6, this projection is as if one were looking up on the thermosphere from below. The thermospheric density shows the maximum and minimum in the postnoon sector (∼1400 MLT) and early morning sector (∼0400 MLT), respectively. Density patterns having the postnoon maximum and early morning minimum at high latitudes have been seen in previous studies [e.g., *Jacchia and Slowley*, 1968; *Liu et al.*, 2005].

[11] Figure 5 shows the average thermospheric total mass density distributions at 400 km for IMF ($\overline{B}_y$, $\overline{B}_z$) values of (−4.4, 0.0), (+4.4, 0.0), (0.0, −3.4), and (0.0, +3.4) nT. For all IMF conditions, there is the classic picture of total mass density, reaching a maximum in the postnoon sector, and a minimum in the early morning sector. And large thermospheric density peaks are clearly visible in the cusp region around noon and −75° magnetic latitude. This feature and its strengthening with increasing magnetic activity have also been seen in previous studies [*Lühr et al.*, 2004; *Liu et al.*, 2005; *Rentz and Lühr*, 2008]. In Figure 5, particularly, it is found that the enhanced thermospheric density near the cusp is most pronounced when the IMF $\overline{B}_z$ is negative. The

**Table 1.** IMF Reference Values and Selection Criteria for Data Subsets

| | Reference IMF | | |
|---|---|---|---|
| Subset | $\overline{B}_y$ | $\overline{B}_z$ | Data Selection Criterion |
| 1 | 0 | 0 | $(\overline{B}_y/6.223)^2 + (\overline{B}_z/4.808)^2 < 1$ |
| 2 | −4.4 | 0 | $\overline{B}_y < -0.647\lvert\overline{B}_z\rvert$ |
| 3 | 4.4 | 0 | $\overline{B}_y > 0.647\lvert\overline{B}_z\rvert$ |
| 4 | 0 | −3.4 | $\overline{B}_z < -0.386\lvert\overline{B}_y\rvert$ |
| 5 | 0 | 3.4 | $\overline{B}_z > 0.386\lvert\overline{B}_y\rvert$ |

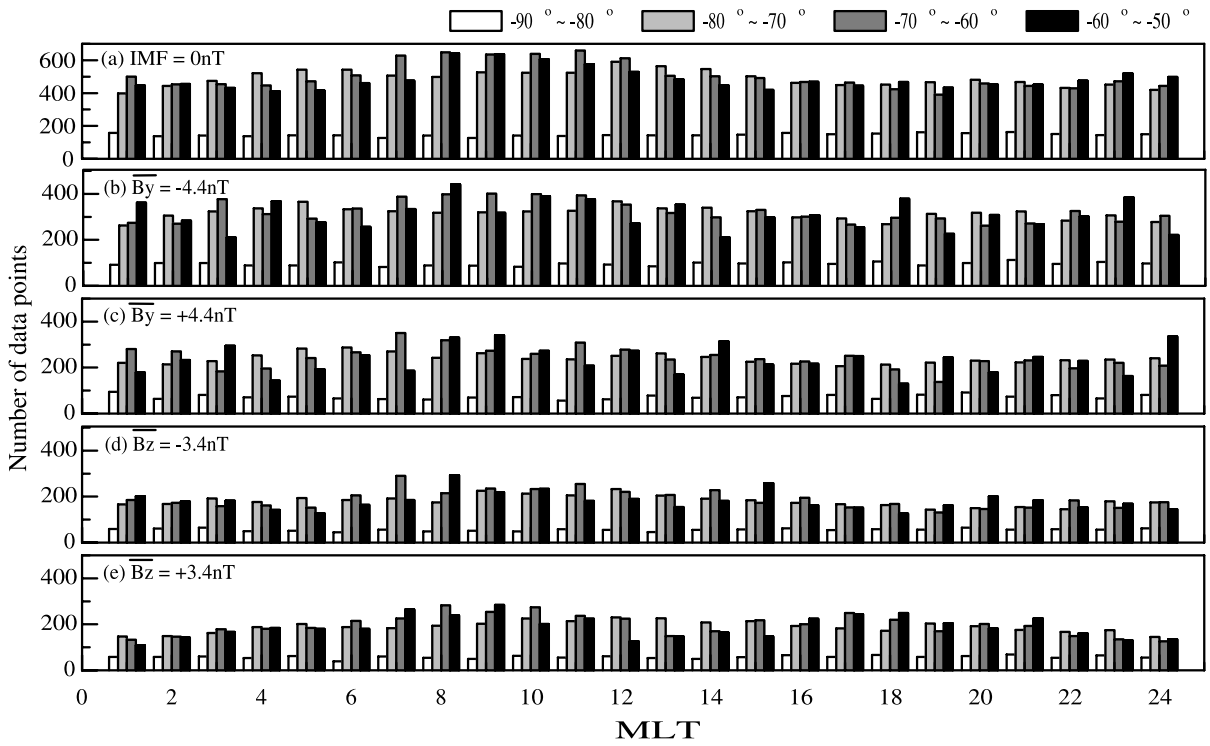


**Figure 3.** Number of CHAMP observations for each magnetic latitudinal range of 10° for IMF ($\overline{B}_y$, $\overline{B}_z$) values of (a) (0.0, 0.0), (b) (−4.4, 0.0), (c) (+4.4, 0.0), (d) (0.0, −3.4), and (e) (0.0, +3.4) nT during 17 October 2001 through 24 February 2002 versus magnetic local time (MLT).

highest thermospheric densities are 16.56 × $10^{-12}$ kg $m^{-3}$ near the cusp region at 400 km altitude for negative $\overline{B}_z$. The densities poleward of −60° tend to be weakest when $\overline{B}_z$ is positive. The densities poleward of −60° also tend to be stronger when $\overline{B}_y$ is negative than when it is positive. In particular, the thermospheric densities for negative $\overline{B}_y$ show larger values around the noon sector and in the early morning hours including the dawn side than when $\overline{B}_y$ is positive.

[12] As known well, the main source driving the variation of the thermospheric density is solar radiation. Although not shown here, the correlation between the solar radiation proxy F10.7 and the total mass density from MSIS00 is high. So by subtracting the densities from MSIS00 from the CHAMP observations, we can consider the nonsolar radiation effect. Then by considering the difference thermospheric densities, obtained by subtracting values with zero IMF (for subset 1) from those with nonzero IMF (for subsets 2–5), we can emphasize the IMF dependency in order to examine more closely how the thermospheric densities are influenced by the orientation of the IMF. Figure 6 shows the difference of thermospheric densities at 400 km over southern hemisphere high latitudes for the four IMF ($\overline{B}_y$, $\overline{B}_z$) values. As shown in Figure 6, the thermospheric density variation patterns in the high latitudes depend on the orientation of the IMF. The difference densities for negative $\overline{B}_y$ show an increase in almost the whole polar regions except for the dusk sector. In particular, there are significantly enhanced densities in the early morning hours including the dawn side and around noon when $\overline{B}_y$ is negative. The positive-$\overline{B}_y$ difference densities have opposite signs from those for negative $\overline{B}_y$. In other words, under the positive-$\overline{B}_y$ condition, although there is an increase of difference density in the afternoon including the dusk side, there is a significant decrease in the early morning hours including the dawn side and around noon equatorward of −70°. The difference of the thermospheric densities for negative $\overline{B}_z$ shows a strong enhancement in the cusp region and premidnight sector with maximum value of 3.49 × $10^{-12}$ kg $m^{-3}$ around the cusp region, but decreases in the dawn sector. In the dusk sector, although densities are not significantly enhanced, those values are relatively larger than those in the dawn sector. The positive-$\overline{B}_z$ difference densities show decreases generally, although there are weak increases on the dawn side and evening sector. The negative-$\overline{B}_z$ difference densities are more significant than the

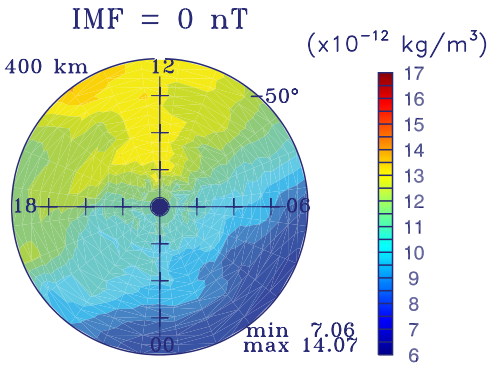


**Figure 4.** The thermospheric densities at 400 km altitude over the southern hemisphere for zero IMF (Subset 1) from CHAMP data.

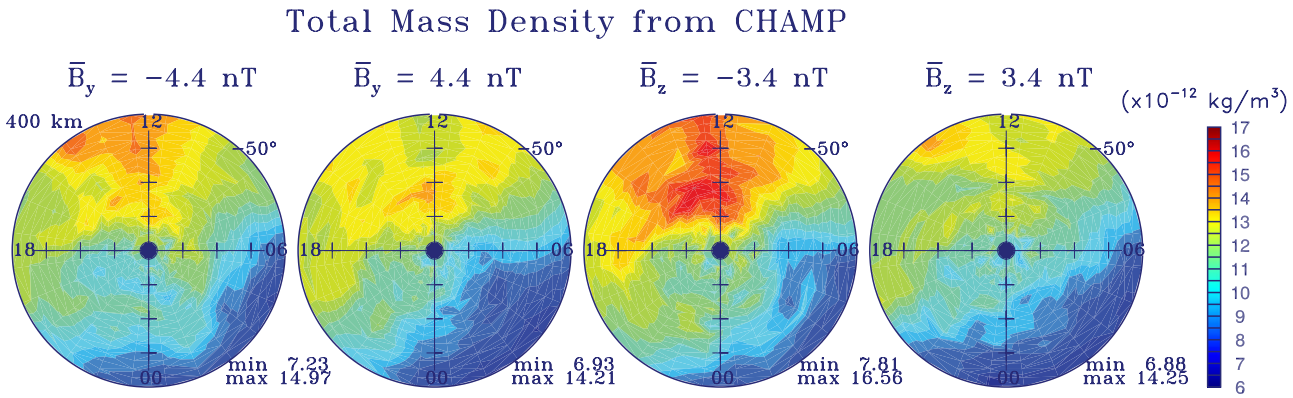


**Figure 5.** The thermospheric densities at 400 km altitude over the southern hemisphere for IMF ($\overline{B}_y$, $\overline{B}_z$) values of (left to right) (−4.4, 0.0), (+4.4, 0.0), (0.0, −3.4), and (0.0, +3.4) nT from CHAMP observations.

positive-$\overline{B}_z$ difference densities, indicating that negative $\overline{B}_z$ has a stronger effect on the thermospheric density than does positive $\overline{B}_z$.

[13] A possible interpretation for different neutral density patterns for different IMF conditions is that the density around the dawn and dusk sectors can be strongly determined by thermospheric winds, which are associated with the ionospheric convection and vary strongly with respect to the direction of IMF [*Crowley et al.*, 2006; *Richmond et al.*, 2003; *Kwak et al.*, 2007]. The IMF effect on the winds is stronger in summer than winter [*Kwak and Richmond*, 2007; *Lühr et al.*, 2007]. Geostrophic adjustment theory, as it applies to the thermosphere [e.g., *Larsen and Mikkelsen*, 1983; *Walterscheid and Boucher*, 1984], indicates that winds and horizontal pressure gradients tend to be linked, such that a cyclonic wind vortex tends to have a low pressure and density at its center, while an anticyclonic vortex tends to have a high pressure and density at its center. This link is apparent in the force analysis of *Kwak et al.* [2007]. Additionally, density variations can be influenced by the local heating associated with ionospheric currents, which vary with IMF conditions, especially in auroral and cusp regions [*Lühr et al.*, 2004; *Neubert and Christiansen*, 2003].

[14] *Crowley et al.* [2006] examined the effect of the IMF $B_y$ component on thermospheric composition and density at 140 and 200 km at high and middle latitudes in the northern hemisphere by using numerical experiments. Their simulations showed a stronger cyclonic wind vortex and lower density on the dawn side of the polar cap for $B_y$-negative than for $B_y$-positive. If applied in the southern hemisphere, where the difference between effects of $B_y$-positive and $B_y$-negative tend to be opposite to those in the northern hemisphere, we would expect $B_y$-positive to drive a more cyclonic wind and a lower neutral density on the dawn side of the polar cap than $B_y$-negative. This generally agrees with the density observations in Figure 6 and with the wind observations presented by *Richmond et al.* [2003] for altitudes above 140 km and by *Förster et al.* [2008] for altitudes around 400 km. Similarly, the dawnside minimum difference density around −70° for negative $\overline{B}_z$, and maximum difference density for positive $\overline{B}_z$, are related to the strength of the cyclonic vortex there seen in the results of *Richmond et al.* [2003] and *Förster et al.* [2008]. In contrast, the difference densities around 1800 MLT are not much larger for negative $\overline{B}_z$ than for positive $\overline{B}_z$, despite the fact that the dusk sector anticyclonic winds shown by *Richmond et al.* [2003] and *Förster et al.* [2008] are considerably stronger for negative $\overline{B}_z$ than for positive $\overline{B}_z$. The possible reason can be that the horizontal advection of momentum, or centrifugal force, is strongly divergent in the dusk sector for $\overline{B}_z$ negative, reducing the need for an

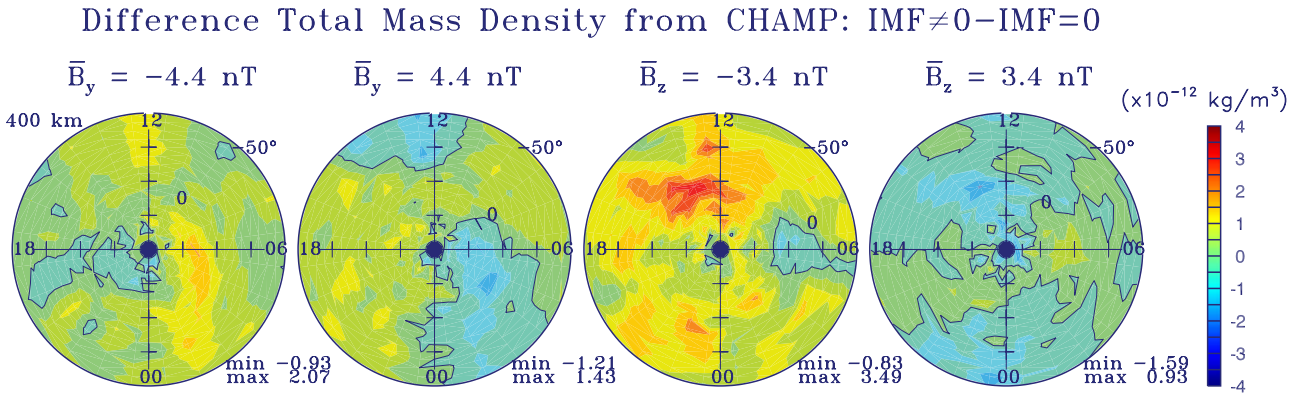


**Figure 6.** Difference densities at 400 km altitude over the southern summer hemisphere for IMF ($\overline{B}_y$, $\overline{B}_z$) values of (left to right) (−4.4, 0.0), (+4.4, 0.0), (0.0, −3.4), and (0.0, +3.4) nT. These are obtained from subsets 2−5, respectively, by subtracting the IMF = 0 densities of Subset 1.

outward pressure gradient force to help balance the Coriolis force [*Kwak et al.*, 2007].

[15] From their results, *Lühr et al.* [2004] suggested Joule heating due to very intense small-scale Field Aligned Currents (FACs) near the cusp region at a lower level causes upwelling and enhanced neutral mass densities at a higher level. In particular, *Neubert and Christiansen* [2003] pointed out that small-scale FACs are strongest in the cusp region when the IMF is strongly southward, which may explain why the strongest thermospheric density peaks near the cusp region occur for negative $\overline{B}_z$. Recently, it has been shown by *Rentz and Lühr* [2008] that the increased positive anomaly in cusp density is detected for about an hour after the enhancement of the merging electric fields, which are proportional to amplitude of southward IMF.

## 4. Summary and Conclusion

[16] In this study we have carried out the systematic analysis of observed IMF $B_y$ and $B_z$ influences on the thermospheric density by using the high-latitude southern summer thermospheric total mass density near 400 km altitude, derived from the high-accuracy accelerometer on board the CHAMP spacecraft during 17 October 2001 through 24 February 2002 centered on the December solstice.

[17] This study shows that the thermospheric density distribution depends on the orientation of the IMF: The densities poleward of $-60^\circ$ tend to be strongest when $\overline{B}_z$ is negative, and stronger when $\overline{B}_y$ is negative than when it is positive. A thermospheric density peak in the cusp region is most pronounced when $\overline{B}_z$ is negative. The densities poleward of $-60^\circ$ tend to be weakest when $\overline{B}_z$ is positive. In particular, the difference densities, which are obtained by subtracting values for zero IMF from those for nonzero IMF, show a significant IMF dependence as follows: The difference density for negative $B_y$ shows significantly enhanced values in the early morning hours and hours around dawn, as well as a smaller enhancement around noon, but reduced values in the premidnight and dusk sectors. For positive $B_y$ the difference densities are opposite to those for negative $B_y$. The difference densities for negative $B_z$ show general enhancements at most locations, with a significant increase in the cusp region, but show a small decrease in the dawn sector.

[18] From previous studies referenced in section 3 and this study we suggest that the IMF variations of high-latitude thermospheric density, especially in the dawn and dusk sectors, can be strongly determined by thermospheric winds, which are associated with the ionospheric convection and vary strongly with respect to the direction of the IMF. We also suggest that the density variations, especially in auroral and cusp regions, are also influenced by the local heating associated with ionospheric currents, which vary with IMF conditions. The heating may generate upward neutral motion and cause an increase of total mass density. However, further study is needed to determine the sources responsible for driving the thermospheric densities and their IMF $B_z$ and $B_y$ variations. Numerical experiments using model simulations can provide insight into these sources. A future paper will conduct and analyze numerical experiments with the NCAR TIE-GCM.

[19] **Acknowledgments.** This work was supported by the "Development of Korean Space Weather Center," the project of KASI, the KASI basic research fund, and the Korea Research Foundation Grant (KRF-2005-070-C00059). This work was also supported in part by NASA Living with a Star grant NNH05AB54I and AFOSR contract FA9550-08-C-0046. The National Center for Atmospheric Research is sponsored by the National Science Foundation. Yue Deng's effort was supported by NSF through grant ATM-0823689 andby University of Colorado through a CIRES fellowship. J.M.F. acknowledges support under grant ATM-0719480 from the National Science Foundation as part of the Space Weather Program and under award FA9550-07-1-0565 through the AFOSR MURI Program. One of authors (K.-H. Kim) has been supported by the WCU grant (R31-10016) funded by the Korean Ministry of Education, Science and Technology. We are grateful to H. Lühr for his insightful discussions.

[20] Zuyin Pu thanks the reviewers for their assistance in evaluating this paper.

## References

Bruinsma, S., D. Tamagnan, and R. Biancale (2004), Atmospheric densities derived from CHAMP/STAR accelerometer observations, *Planet. Space Sci.*, *52*, 297–312, doi:10.1016/j.pss.2003.11.004.

Bruinsma, S., J. M. Forbes, R. S. Nerem, and X. Zhang (2006), Thermosphere density response to the 20–21 November 2003 solar and geomagnetic storm from CHAMP and GRACE accelerometer data, *J. Geophys. Res.*, *111*, A06303, doi:10.1029/2005JA011284.

Burns, A. G., T. L. Killeen, and R. G. Roble (1991), A theoretical study of thermospheric composition perturbations during an impulsive geomagnetic storm, *J. Geophys. Res.*, *96*, 14,153–14,167, doi:10.1029/91JA00678.

Burns, A. G., T. L. Killeen, G. R. Carignan, and R. G. Roble (1995a), Large enhancements in the $O/N_2$ ratio in the evening sector of the winter hemisphere during geomagnetic storms, *J. Geophys. Res.*, *100*, 14,661–14,671, doi:10.1029/94JA03235.

Burns, A. G., T. L. Killeen, W. Deng, G. R. Carignan, and R. G. Roble (1995b), Geomagnetic storm effects in the low- to middle-latitude upper thermosphere, *J. Geophys. Res.*, *100*, 14,673–14,691, doi:10.1029/94JA03232.

Crowley, G., T. J. Immel, C. L. Hackert, J. Craven, and R. G. Roble (2006), Effect of IMF $B_y$ on thermospheric composition at high and middle latitude: 1. Numerical experiments, *J. Geophys. Res.*, *111*, A10311, doi:10.1029/2005JA011371.

Forbes, J. M., R. Gonzalez, F. A. Marcos, D. Revelle, and H. Parish (1996), Magnetic storm response of lower thermosphere density, *J. Geophys. Res.*, *101*, 2313–2319, doi:10.1029/95JA02721.

Förster, M., S. Rentz, W. Köhler, H. Liu, and S. E. Haaland (2008), IMF dependence of high-latitude thermospheric wind pattern derived from CHAMP cross-track measurements, *Ann. Geophys.*, *26*, 1581–1595.

Foster, J. C., J. M. Holt, R. G. Musgrove, and D. S. Evans (1986), Solar wind dependence of high-latitude convection and precipitation, in *Solar Wind-Magnetosphere Coupling*, edited by Y. Kamide and J. A. Slavin, pp. 477–494, Terra Sci., Tokyo.

Fuller-Rowell, T. J., M. V. Codrescu, R. J. Moffett, and S. Quegan (1994), Response of the thermosphere and ionosphere to geomagnetic storms, *J. Geophys. Res.*, *99*, 3893–3914, doi:10.1029/93JA02015.

Fuller-Rowell, T. J., M. V. Codrescu, H. Rishbeth, R. J. Moffett, and S. Quegan (1996), On the seasonal response of the thermosphere and ionosphere to geomagnetic storms, *J. Geophys. Res.*, *101*, 2343–2353, doi:10.1029/95JA01614.

Heppner, J. P. (1972), Polar cap electric field distributions related to the interplanetary magnetic field direction, *J. Geophys. Res.*, *77*, 4877–4887, doi:10.1029/JA077i025p04877.

Heppner, J. P., and N. C. Maynard (1987), Empirical high-latitude electric field models, *J. Geophys. Res.*, *92*, 4467–4489, doi:10.1029/JA092iA05p04467.

Hernandez, G., F. G. McCormac, and R. W. Smith (1991), Austral thermospheric wind circulation and interplanetary magnetic field orientation, *J. Geophys. Res.*, *96*, 5777–5783, doi:10.1029/90JA02458.

Jacchia, L. G., and J. W. Slowley (1968), Diurnal and seasonal latitudinal variations in the upper atmosphere, *Planet. Space Sci.*, *16*, 509–524, doi:10.1016/0032-0633(68)90165-7.

Killeen, T. L., R. A. Heelis, P. B. Hays, N. W. Spencer, and W. B. Hanson (1985), Neutral motions in the polar thermosphere for northward interplanetary magnetic field, *Geophys. Res. Lett.*, *12*, 159–162, doi:10.1029/GL012i004p00159.

Killeen, T. L., Y.-I. Won, R. J. Niciejewski, and A. G. Burns (1995), Upper thermosphere winds and temperatures in the geomagnetic polar cap: Solar cycle, geomagnetic activity, and interplanetary magnetic field dependencies, *J. Geophys. Res.*, *100*, 21,327–21,342, doi:10.1029/95JA01208.

Kwak, Y.-S., and A. D. Richmond (2007), An analysis of the momentum forcing in the high-latitude lower thermosphere, *J. Geophys. Res.*, *112*, A01306, doi:10.1029/2006JA011910.

Kwak, Y.-S., A. D. Richmond, and R. G. Roble (2007), Dependence of the high-latitude lower thermospheric momentum forcing on the interplanetary magnetic field, *J. Geophys. Res.*, *112*, A06316, doi:10.1029/2006JA012208.

Larsen, M. F., and I. S. Mikkelsen (1983), The dynamic response of the high-latitude thermosphere and geostrophic adjustment, *J. Geophys. Res.*, *88*, 3158–3168, doi:10.1029/JA088iA04p03158.

Liu, H., and H. Lühr (2005), Strong disturbance of the upper thermospheric density due to magnetic storms: CHAMP observations, *J. Geophys. Res.*, *110*, A09S29, doi:10.1029/2004JA010908.

Liu, H., H. Lühr, V. Henize, and W. Köhler (2005), Global distribution of the thermospheric total mass density derived from CHAMP, *J. Geophys. Res.*, *110*, A04301, doi:10.1029/2004JA010741.

Lühr, H., M. Rother, W. Köhler, P. Ritter, and L. Grunwaldt (2004), Thermospheric up-welling in the cusp region: Evidence from CHAMP observations, *Geophys. Res. Lett.*, *31*, L06805, doi:10.1029/2003GL019314.

Lühr, H., S. Rentz, P. Ritter, H. Liu, and K. Häusler (2007), Average thermospheric wind pattern over the polar regions, as observed by CHAMP, *Ann. Geophys.*, *25*, 1093–1101.

Mayr, H. G., and H. Volland (1973), A two-component model of the variations in the thermospheric composition, *J. Atmos. Terr. Phys.*, *35*, 669–680.

McCormac, F. G., and R. W. Smith (1984), The influence of the interplanetary magnetic field Y component on ion and neutral motions in the polar thermosphere, *Geophys. Res. Lett.*, *11*, 935–938, doi:10.1029/GL011i009p00935.

McCormac, F. G., T. L. Killeen, E. Gombosi, P. B. Hays, and N. W. Spencer (1985), Configuration of the high-latitude thermosphere neutral circulation for IMF $B_y$ negative and positive, *Geophys. Res. Lett.*, *12*, 155–158, doi:10.1029/GL012i004p00155.

McCormac, F. G., T. L. Killeen, and J. P. Thayer (1991), The influence of IMF $B_y$ on the high-latitude thermospheric circulation during northward IMF, *J. Geophys. Res.*, *96*, 115–128.

McHarg, M., F. Chun, D. Knipp, G. Lu, B. Emery, and A. Ridley (2005), High-latitude Joule heating response to IMF inputs, *J. Geophys. Res.*, *110*, A08309, doi:10.1029/2004JA010949.

Meriwether, J. W., Jr., and P. Shih (1987), On the nighttime signatures of thermospheric winds observed at Sondrestrom, Greenland, as correlated with interplanetary magnetic field parameters, *Ann. Geophys.*, *5A*, 329–336.

Miller, N. J., L. H. Brace, N. W. Spencer, and G. R. Carignan (1990), DE 2 observations of disturbances in the upper atmosphere during a geomagnetic storm, *J. Geophys. Res.*, *95*, 21,017–21,031, doi:10.1029/JA095iA12p21017.

Neubert, T., and F. Christiansen (2003), Small-scale, field-aligned currents at the top-side ionosphere, *Geophys. Res. Lett.*, *30*(19), 2010, doi:10.1029/2003GL017808.

Niciejewski, R. J., T. L. Killeen, R. M. Johnson, and J. P. Thayer (1992), The behavior of the high-latitude *F* region neutral thermosphere in relation to IMF parameters, *Adv. Space Res.*, *12*(6), 215–218, doi:10.1016/0273-1177(92)90058-6.

Niciejewski, R. J., T. L. Killeen, and Y. Won (1994), Observations of neutral winds in the polar cap during northward IMF, *J. Atmos. Terr. Phys.*, *56*, 285–295, doi:10.1016/0021-9169(94)90036-1.

Picone, J. M., A. E. Hedin, D. P. Drob, and A. C. Aikin (2002), NRLMSISE-00 empirical model of the atmosphere: Statistical comparisons and scientific issues, *J. Geophys. Res.*, *107*(A12), 1468, doi:10.1029/2002JA009430.

Prölss, G. W. (1980), Magnetic storm associated perturbations of the upper atmosphere: Recent results obtained by satellite-borne gas analyzers, *Rev. Geophys.*, *18*, 183–202, doi:10.1029/RG018i001p00183.

Rees, D., and T. J. Fuller-Rowell (1989), The response of the thermosphere and ionosphere to magnetospheric forcing, *Philos. Trans. R. Soc. London, Ser. A*, *328*, 139–171, doi:10.1098/rsta.1989.0029.

Rees, D., and T. J. Fuller-Rowell (1990), Modelling of *E* region auroral winds, *Adv. Space Res.*, *10*(6), 197–213, doi:10.1016/0273-1177(90)90254-W.

Rentz, S., and H. Lühr (2008), Climatology of the cusp-related thermospheric mass density anomaly, as derived from CHAMP observations, *Ann. Geophys.*, *26*, 2807–2823.

Richmond, A. D. (1995), Ionospheric electrodynamics using Magnetic Apex Coordinates, *J. Geomagn. Geoelectr.*, *47*, 191–212.

Richmond, A. D., C. Lathuillère, and S. Vennerstroem (2003), Winds in the high-latitude lower thermosphere: Dependence on the interplanetary magnetic field, *J. Geophys. Res.*, *108*(A2), 1066, doi:10.1029/2002JA009493.

Ruohoniemi, J. M., and R. A. Greenwald (1996), Statistical patterns of high-latitude convection obtained from Goose Bay HF radar observations, *J. Geophys. Res.*, *101*, 21,743–21,763, doi:10.1029/96JA01584.

Sica, R. J., G. Hernandez, B. A. Emery, R. G. Roble, R. W. Smith, and M. H. Rees (1989), The control of auroral zone dynamics and thermodynamics by the interplanetary magnetic field dawn-dusk (*Y*) component, *J. Geophys. Res.*, *94*, 11,921–11,932, doi:10.1029/JA094iA09p11921.

Sutton, E. K., J. M. Forbes, and R. S. Nerem (2005), Global thermospheric neutral density and wind response to the severe 2003 geomagnetic storms from CHAMP accelerometer data, *J. Geophys. Res.*, *110*, A09S40, doi:10.1029/2004JA010985.

Sutton, E. K., R. S. Nerem, and J. M. Forbes (2007), Atmospheric density and wind measurements deduced from accelerometer data, *J. Spacecr. Rockets*, *44*(6), doi:10.2514/1.28641.

Thayer, J. P, T. L. Killeen, F. G. McCormac, C. R. Tschan, J.-J. Ponthieu, and N. W. Spencer (1987), Thermospheric neutral wind signatures dependent on the east-west component of the interplanetary magnetic field for northern and southern hemispheres as measured from Dynamics Explorer-2, *Ann. Geophys.*, *5A*, 363–368.

Walterscheid, R. L., and D. J. Boucher (1984), A simple model of the transient response of the thermosphere to impulsive forcing, *J. Atmos. Sci.*, *41*, 1062–1072, doi:10.1175/1520-0469(1984)041<1062:ASMOTT>2.0.CO;2.

Weimer, D. R. (1995), Models of high-latitude electric potentials derived with a least error fit of spherical harmonic coefficients, *J. Geophys. Res.*, *100*, 19,595–19,607, doi:10.1029/95JA01755.

Weimer, D. R. (2001), An improved model of ionospheric electric potentials including substorm perturbations and application to the Geospace Environment Modeling November 24, 1996, event, *J. Geophys. Res.*, *106*, 407–416, doi:10.1029/2000JA000604.

Won, Y. (1994), Studies of thermospheric neutral winds utilizing ground-based optical and radar measurements, Ph.D. thesis, Univ. of Mich., Ann Arbor.

Zhang, X. X., C. Wang, T. Chen, Y. L. Wang, A. Tan, T. S. Wu, G. A. Germany, and W. Wang (2005), Global patterns of Joule heating in the high-latitude ionosphere, *J. Geophys. Res.*, *110*, A12208, doi:10.1029/2005JA011222.

Y. Deng, Space Weather Prediction Center, NOAA, Department of Commerce Boulder Labs, 325 Broadway, Boulder, CO 80305, USA. (yue.deng@noaa.gov)

J. M. Forbes, Department of Aerospace Engineering Sciences, University of Colorado, 1000 Engineering, Boulder, CO 80309, USA. (forbes@colorado.edu)

K.-H. Kim, Department of Astronomy and Space Science, Kyung Hee University, 1 Seocheon-dong, Giheung-gu, Yongin-si, Gyeonggi-do, 446-701, South Korea. (khan@khu.ac.kr)

Y.-S. Kwak, Division of Space Astronomy, Korea Astronomy and Space Science Institute, 61-1, Hwaam-Dong, Yuseong-Gu, Daejeon, 305-348, Korea. (yskwak@kasi.re.kr)

A. D. Richmond, High Altitude Observatory, National Center for Atmospheric Research, P.O. Box 3000, Boulder, CO 80307, USA. (richmond@hao.ucar.edu)